Crystal structure of diclazuril, $C_{17}H_9Cl_3N_4O_2$

James A. Kaduk,[1,2,a] Stacy Gates-Rector,[3] and Thomas N. Blanton[3]
[1]*Illinois Institute of Technology, 3101 S. Dearborn St., Chicago, IL 60616, USA*
[2]*North Central College, 131 S. Loomis St., Naperville, IL 60540, USA*
[3]*ICDD, 12 Campus Blvd., Newtown Square, PA 19073-3273, USA*

(Received 28 June 2022; accepted 12 September 2022)

The crystal structure of diclazuril has been solved and refined using synchrotron X-ray powder diffraction data, and optimized using density functional theory techniques. Diclazuril crystallizes in space group $P2_1/a$ (#14) with $a = 27.02080(18)$, $b = 11.42308(8)$, $c = 5.36978(5)$ Å, $\beta = 91.7912(7)°$, $V = 1656.629(15)$ Å^3, and $Z = 4$. The crystal structure consists of layers of molecules parallel to the *ac*-plane. A strong N–H···O hydrogen bond links the molecules into dimers along the *a*-axis with a graph set *R2,2(8)*. The powder pattern has been submitted to ICDD for inclusion in the Powder Diffraction File™ (PDF®). [doi:10.1017/S0885715622000410]

Key words: diclazuril, Protazil®, powder diffraction, Rietveld refinement, density functional theory

I. INTRODUCTION

Diclazuril (sold under the brand names Protazil®, Vecoxan, and Clinacox) is an FDA-approved veterinary pharmaceutical (in the US) for equine protozoal myeloencephalitis (EPM) in horses and as a coccidiostat in broiler chickens. The systematic name (CAS Registry Number 101831-37-2) is 2-(4-chlorophenyl)-2-[2,6-dichloro-4-(3,5-dioxo-1,2,4-triazin-2-yl)phenyl]acetonitrile. A two-dimensional molecular diagram is shown in Figure 1. Some studies of diclazuril are summarized in Chapman *et al.* (2013), but we are unaware of any published X-ray powder diffraction data on this compound.

This work was carried out as part of a project (Kaduk *et al.*, 2014) to determine the crystal structures of large-volume commercial pharmaceuticals, and include high-quality powder diffraction data for them in the Powder Diffraction File (Gates-Rector and Blanton, 2019).

II. EXPERIMENTAL

Diclazuril was a commercial reagent, purchased from TargetMol (Lot #112009), and was used as-received. The white powder was packed into a 1.5 mm diameter Kapton capillary, and rotated during the measurement at ~50 Hz. The powder pattern was measured at 295 K at beamline 11-BM (Antao *et al.*, 2008; Lee *et al.*, 2008; Wang *et al.*, 2008) of the Advanced Photon Source at Argonne National Laboratory using a wavelength of 0.458208(2) Å from 0.5 to 50° 2θ with a step size of 0.0009984375 and a counting time of 0.1 s per step. The high-resolution powder diffraction data were collected using twelve silicon crystal analyzers that allow for high angular resolution, high precision, and accurate peak positions. A silicon (NIST SRM 640c) and alumina (SRM 676a) standard (ratio Al_2O_3:Si = 2:1 by weight) was used to calibrate the instrument and refine the monochromatic wavelength used in the experiment.

The pattern was indexed using N-TREOR (Altomare *et al.*, 2013) on a primitive monoclinic cell with $a = 27.02114$, $b = 11.43736$, $c = 5.37083$ Å, $\beta = 91.810°$, $V = 1659.0$ Å^3, and $Z = 4$. A reduced cell search in the Cambridge Structural Database (Groom *et al.*, 2016) with the chemistry H, C, Cl, N, and O only yielded one hit, but no structures of diclazuril. The suggested space group was $P2_1/a$, which was confirmed by successful solution and refinement of the structure. A diclazuril molecule was downloaded from PubChem (Kim *et al.*, 2019) as Conformer3D_CID_465389.sdf. It was converted to a *.mol2 file using Mercury (Macrae *et al.*, 2020). The structure was solved by Monte Carlo simulated annealing as implemented in EXPO2014 (Altomare *et al.*, 2013).

Rietveld refinement was carried out using GSAS-II (Toby and Von Dreele, 2013). Only the 1.8–30.0° portion of the

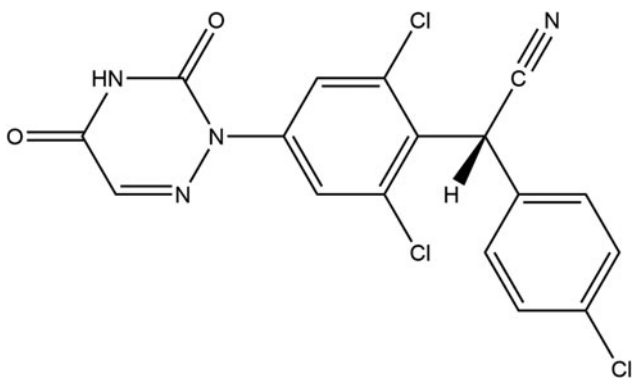

Figure 1. The 2D molecular structure of diclazuril.

[a]Author to whom correspondence should be addressed. Electronic mail: kaduk@polycrystallography.com

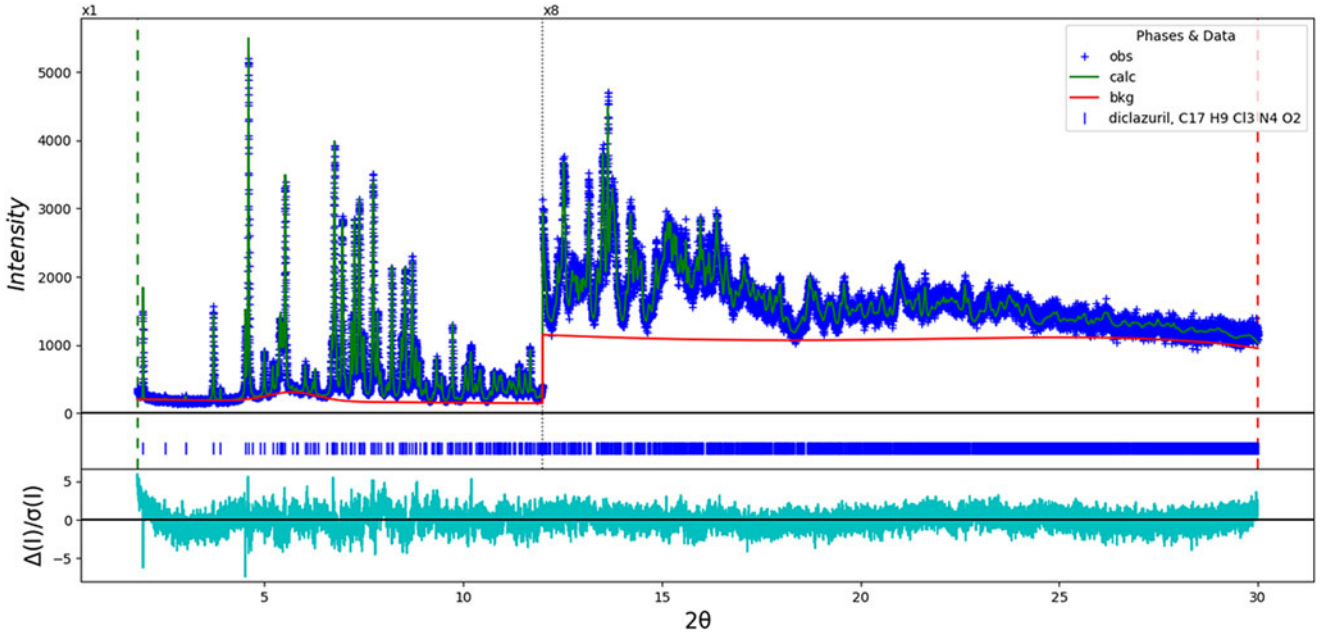

Figure 2. The Rietveld plot for the refinement of diclazuril. The blue crosses represent the observed data points, and the green line is the calculated pattern. The cyan curve is the normalized error plot. The vertical scale has been multiplied by a factor of 8× for $2\theta > 12.0°$. The row of blue tick marks indicates the calculated reflection positions.

pattern was included in the refinement ($d_{min} = 0.885$ Å). All non-H bond distances and angles were subjected to restraints, based on a Mercury/Mogul Geometry Check (Bruno *et al.*, 2004; Sykes *et al.*, 2011). The Mogul average and standard deviation for each quantity were used as the restraint parameters. The restraints contributed 4.2% to the final χ^2. The hydrogen atoms were included in calculated positions, which were recalculated during the refinement using Materials Studio (Dassault, 2021). The U_{iso} of the heavy atoms were grouped by chemical similarity. The U_{iso} for the H atoms were fixed at 1.2× the U_{iso} of the heavy atoms to which they are attached. No preferred orientation model was necessary for this rotated capillary specimen. The peak profiles were described using the generalized microstrain model. The background was modeled using a 6-term shifted Chebyshev polynomial, and a peak at 5.72° 2θ to model the scattering from the Kapton capillary and any amorphous component.

The final refinement of 106 variables using 28 245 observations and 68 restraints yielded the residuals $R_{wp} = 0.0633$ and GOF = 1.16. The largest peak (1.67 Å from C11) and hole (1.77 Å from C22) in the difference Fourier map were 0.31(7) and −0.33(7) eÅ^{-3}, respectively. The largest errors in the difference plot (Figure 2) are very small.

The crystal structure was optimized using density functional techniques as implemented in VASP (Kresse and Furthmüller, 1996) (fixed experimental unit cell) through the MedeA graphical interface (Materials Design, 2016). The calculation was carried out on 16 2.4 GHz processors (each with 4 GB RAM) of a 64-processor HP Proliant DL580 Generation 7 Linux cluster at North Central College. The calculation used the GGA-PBE functional, a plane wave cutoff energy of 400.0 eV, and a k-point spacing of 0.5 Å^{-1} leading to a 3 × 2 × 3 mesh, and took ∼127 h. A single-point density functional calculation (fixed experimental cell) and population analysis were carried out using CRYSTAL17 (Dovesi *et al.*, 2018). The basis sets for the H, C, and O atoms in the calculation were those of Gatti *et al.* (1994), and that for Cl was that of Peintinger *et al.* (2013). The calculations were run on a 3.5 GHz PC using 8 k-points and the B3LYP functional, and took ∼1.8 h.

III. RESULTS AND DISCUSSION

The root-mean-square (rms) Cartesian displacement between the Rietveld-refined and DFT-optimized structures of diclazuril is 0.051 Å (Figure 3). The excellent agreement provides strong evidence that the refined structure is correct (van de Streek and Neumann, 2014). This discussion concentrates on the DFT-optimized structure. The asymmetric unit (with atom numbering) is illustrated in Figure 4. The best view of the crystal structure is down the short c-axis (Figure 5). The crystal structure consists of layers of molecules parallel to the ac-plane.

All of the bond distances and bond angles fall within the normal ranges indicated by a Mercury/Mogul Geometry Check (Macrae *et al.*, 2020). The torsion angles involving rotation about the C13–N6 bond are flagged as unusual. For example, the C16–C13–N6–N7 angle of 74° lies on the tail

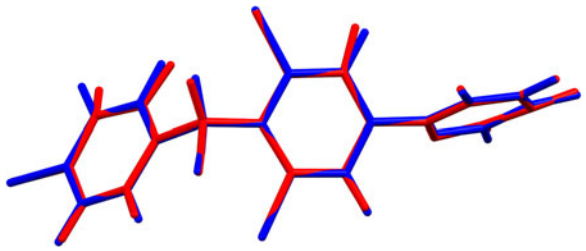

Figure 3. Comparison of the Rietveld-refined (red) and VASP-optimized (blue) structures of diclazuril. The rms Cartesian displacement is 0.051 Å. Image generated using Mercury (Macrae *et al.*, 2020).

https://doi.org/10.1017/S0885715622000410 Published online by Cambridge University Press

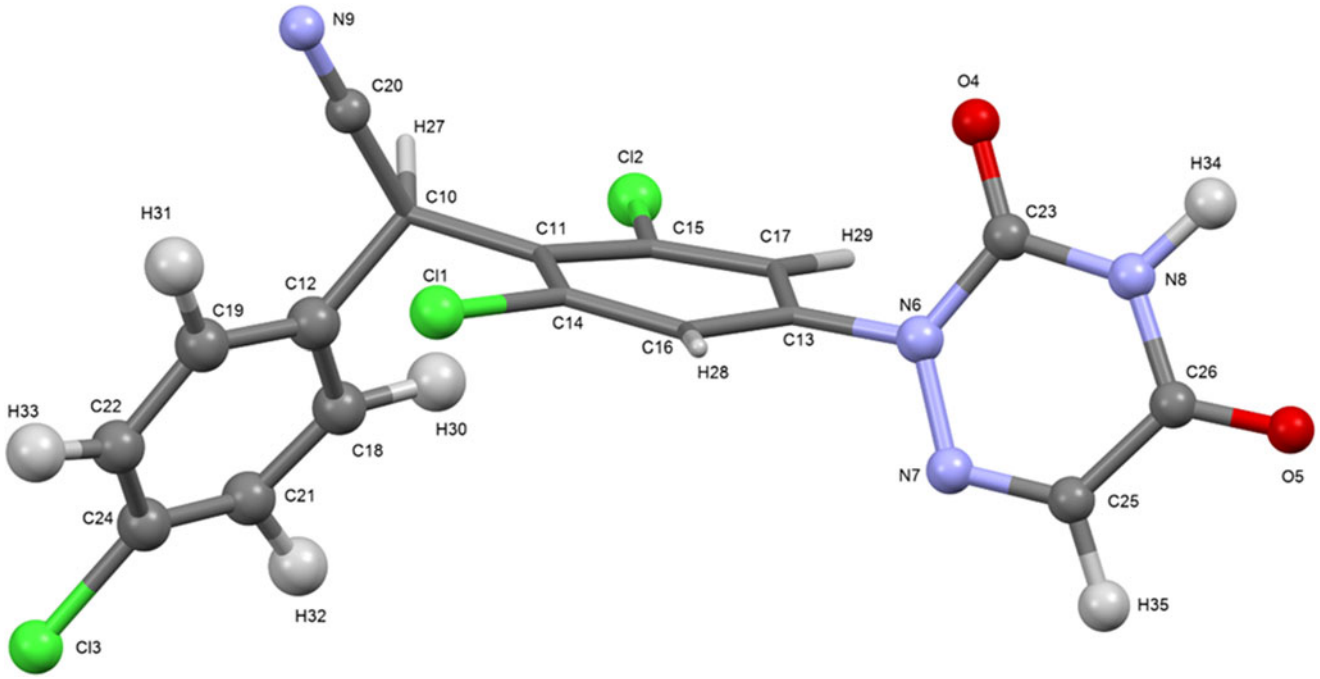

Figure 4. The asymmetric unit of diclazuril, with the atom numbering. The atoms are represented by 50% probability spheroids. Image generated using Mercury (Macrae *et al.*, 2020).

of one part of a bimodal distribution of similar torsion angles, with peaks at ∼40 and ∼140°. These torsion angles indicate the angle between the triazine ring and one of the phenyl rings seems to be slightly unusual.

Quantum chemical geometry optimization of the diclazuril molecule (DFT/B3LYP/6-31G*/water) using Spartan '18 (Wavefunction, 2020) indicated that the observed conformation is 55.9 kcal mol^{-1} higher in energy than the local minimum. The major differences are in the orientations of the outer rings of the molecule. A conformational analysis (MMFF force field) indicates that the minimum-energy conformation is 21.1 kcal mol^{-1} lower in energy, but the

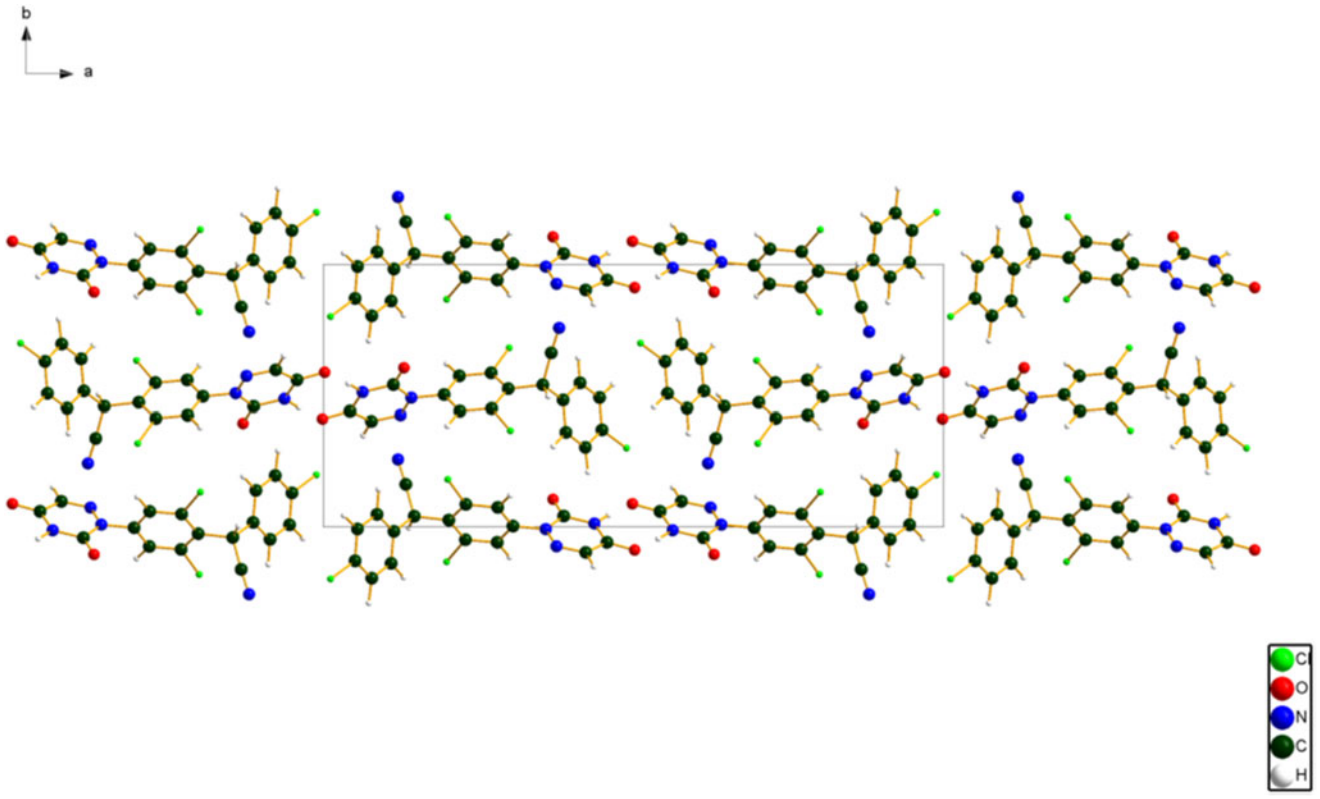

Figure 5. The crystal structure of diclazuril, viewed down the *c*-axis. Image generated using diamond (Crystal Impact, 2022).

https://doi.org/10.1017/S0885715622000410 Published online by Cambridge University Press

TABLE I. Hydrogen bonds (CRYSTAL17) in diclazuril

H-Bond	D-H (Å)	H···A (Å)	D···A (Å)	D-H···A (°)	Overlap (*e*)	*E* (kcal mol^{-1})
N8–H34···O5	1.055	1.697	2.751	176.1	0.079	6.5
C10–H27···Cl2	1.105	2.393[a]	3.061	117.3	0.022	
C22–H23···Cl3	1.090	2.896	3.977	171.5	0.018	
C18–H30···O4	1.091	2.369	3.221	133.7	0.015	
C16–H28···O4	1.090	2.641	3.597	146.0	0.013	
C21–H32···O5	1.090	2.587	3.385	129.4	0.010	

[a]Intramolecular.

molecule folds on itself to make the Cl-containing rings parallel. Intermolecular interactions are thus important in determining the solid-state conformation.

Analysis of the contributions to the total crystal energy of the structure using the Forcite module of Materials Studio (Dassault, 2021) suggests that the intramolecular deformation energy terms are small, but that torsion deformation terms are the largest. The intermolecular energy is dominated by electrostatic attractions, which in this force field analysis include hydrogen bonds. The hydrogen bonds are better analyzed using the results of the DFT calculation.

Hydrogen bonds are prominent in the structure (Table I). The most noteworthy is the strong N8–H34···O5 hydrogen bond, which links the molecules into dimers along the *a*-axis with a graph set *R2,2(8)* (Etter, 1990; Bernstein *et al.*, 1995; Shields *et al.*, 2000). The energy of the N–H···O hydrogen bond was calculated using the correlation of Wheatley and Kaduk (2019). The methyne carbon C10 forms an intramolecular C–H···Cl hydrogen bond. Intermolecular C–H···Cl and C–H···O hydrogen bonds also contribute to the lattice energy.

The volume enclosed by the Hirshfeld surface of diclazuril (Figure 6, Hirshfeld, 1977; Turner *et al.*, 2017) is 406.45 Å^3, 98.14% of 1/4 the unit cell volume. The packing density is thus fairly typical. The only significant-close contacts (red in Figure 6) involve the hydrogen bonds. The volume/non-hydrogen atom is smaller than usual at 15.9 Å^3.

The Bravais–Friedel–Donnay–Harker (Bravais, 1866; Friedel, 1907; Donnay and Harker, 1937) morphology suggests that we might expect elongated morphology for diclazuril, with [001] as the long axis. No preferred orientation model was necessary for this rotated capillary specimen.

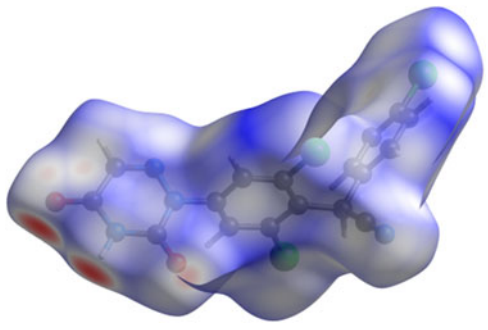

Figure 6. The Hirshfeld surface of diclazuril. Intermolecular contacts longer than the sums of the van der Waals radii are colored blue, and contacts shorter than the sums of the radii are colored red. Contacts equal to the sums of radii are white. Image generated using CrystalExplorer (Turner *et al.*, 2017).

IV. DEPOSITED DATA

The Crystallographic Information Framework (CIF) files containing the results of the Rietveld refinement (including the raw data) and the DFT geometry optimization were deposited with the ICDD. The data can be requested at pdj@icdd.com.

ACKNOWLEDGEMENTS

The use of the Advanced Photon Source at Argonne National Laboratory was supported by the U.S. Department of Energy, Office of Science, Office of Basic Energy Sciences, under Contract No. DE-AC02-06CH11357. This work was partially supported by the International Centre for Diffraction Data. We thank Lynn Ribaud and Saul Lapidus for their assistance in the data collection.

CONFLICT OF INTEREST

The authors have no conflict of interest to declare.

Altomare, A., Cuocci, C., Giacovazzo, C., Moliterni, A., Rizzi, R., Corriero, N., and Falcicchio, A. (**2013**). "EXPO2013: a kit of tools for phasing crystal structures from powder data," J. Appl. Crystallogr. **46**, 1231–1235.

Antao, S. M., Hassan, I., Wang, J., Lee, P. L., and Toby, B. H. (**2008**). "State-of-the-art high-resolution powder X-ray diffraction (HRPXRD) illustrated with Rietveld refinement of quartz, sodalite, tremolite, and meionite," Can. Mineral. **46**, 1501–1509.

Bernstein, J., Davis, R. E., Shimoni, L., and Chang, N. L. (**1995**). "Patterns in hydrogen bonding: functionality and graph set analysis in crystals," Angew. Chem., Int. Ed. Engl. **34**(15), 1555–1573.

Bravais, A. (**1866**). *Etudes Cristallographiques* (Gauthier Villars, Paris).

Bruno, I. J., Cole, J. C., Kessler, M., Luo, J., Motherwell, W. D. S., Purkis, L. H., Smith, B. R., Taylor, R., Cooper, R. I., Harris, S. E., and Orpen, A. G. (**2004**). "Retrieval of crystallographically-derived molecular geometry information," J. Chem. Inf. Sci. **44**, 2133–2144.

Chapman, H. D., Barta, J. R., Blake, D., Gruber, A., Jenkins, M., Smith, N. C., Suo, X., and Tomley, F. M. (**2013**). "A selective review of advances in coccidiosis research," Adv. Parasitol. **83**, 93–171.

Crystal Impact - Dr. H. Putz & Dr. K. Brandenburg (**2022**). Diamond - Crystal and Molecular Structure Visualization. Kreuzherrenstr. 102, 53227 Bonn, Germany. Available at: https://www.crystalimpact.de/diamond.

Dassault Systèmes (**2021**). *Materials Studio 2021* (BIOVIA, San Diego, CA).

Donnay, J. D. H. and Harker, D. (**1937**). "A new law of crystal morphology extending the law of Bravais," Am. Mineral. **22**, 446–447.

Dovesi, R., Erba, A., Orlando, R., Zicovich-Wilson, C. M., Civalleri, B., Maschio, L., Rerat, M., Casassa, S., Baima, J., Salustro, S., and Kirtman, B. (**2018**). "Quantum-mechanical condensed matter simulations with CRYSTAL," WIREs Comput. Mol. Sci. **8**, e1360.

Etter, M. C. (**1990**). "Encoding and decoding hydrogen-bond patterns of organic compounds," Acc. Chem. Res. **23**(4), 120–126.

Friedel, G. (**1907**). "Etudes sur la loi de Bravais," Bull. Soc. Fr. Mineral. **30**, 326–455.

Gates-Rector, S. and Blanton, T. (**2019**). "The Powder Diffraction File: a quality materials characterization database," Powd. Diffr. **39**(4), 352–360.
Gatti, C., Saunders, V. R., and Roetti, C. (**1994**). "Crystal-field effects on the topological properties of the electron-density in molecular crystals - the case of urea," J. Chem. Phys. **101**, 10686–10696.
Groom, C. R., Bruno, I. J., Lightfoot, M. P., and Ward, S. C. (**2016**). "The Cambridge Structural Database," Acta Crystallogr. Sect. B: Struct. Sci., Cryst. Eng. Mater. **72**, 171–179.
Hirshfeld, F. L. (**1977**). "Bonded-atom fragments for describing molecular charge densities," Theor. Chem. Acta **44**, 129–138.
Kaduk, J. A., Crowder, C. E., Zhong, K., Fawcett, T. G., and Suchomel, M. R. (**2014**). "Crystal structure of atomoxetine hydrochloride (Strattera), $C_{17}H_{22}NOCl$," Powd. Diffr. **29**(3), 269–273.
Kim, S., Chen, J., Cheng, T., Gindulyte, A., He, J., He, S., Li, Q., Shoemaker, B. A., Thiessen, P. A., Yu, B., Zaslavsky, L., Zhang, J., and Bolton, E. E. (**2019**). "PubChem 2019 update: improved access to chemical data," Nucleic Acids Res. **47**(D1), D1102–D1109. doi:10.1093/nar/gky1033.
Kresse, G. and Furthmüller, J. (**1996**). "Efficiency of ab-initio total energy calculations for metals and semiconductors using a plane-wave basis set," Comput. Mater. Sci. **6**, 15–50.
Lee, P. L., Shu, D., Ramanathan, M., Preissner, C., Wang, J., Beno, M. A., Von Dreele, R. B., Ribaud, L., Kurtz, C., Antao, S. M., Jiao, X., and Toby, B. H. (**2008**). "A twelve-analyzer detector system for high-resolution powder diffraction," J. Synchrotron Radiat. **15**(5), 427–432.
Macrae, C. F., Sovago, I., Cottrell, S. J., Galek, P. T. A., McCabe, P., Pidcock, E., Platings, M., Shields, G. P., Stevens, J. S., Towler, M., and Wood, P. A. (**2020**). "*Mercury 4.0*: from visualization to design and prediction," J. Appl. Crystallogr. **53**, 226–235.
Materials Design (**2016**). *MedeA 2.20.4* (Materials Design Inc., Angel Fire, NM).
Peintinger, M. F., Vilela Oliveira, D., and Bredow, T. (**2013**). "Consistent Gaussian basis sets of triple-zeta valence with polarization quality for solid-state calculations," J. Comput. Chem. **34**, 451–459.
Shields, G. P., Raithby, P. R., Allen, F. H., and Motherwell, W. S. (**2000**). "The assignment and validation of metal oxidation states in the Cambridge Structural Database," Acta Crystallogr. Sec. B: Struct. Sci. **56**(3), 455–465.
Sykes, R. A., McCabe, P., Allen, F. H., Battle, G. M., Bruno, I. J., and Wood, P. A. (**2011**). "New software for statistical analysis of Cambridge Structural Database data," J. Appl. Crystallogr. **44**, 882–886.
Toby, B. H. and Von Dreele, R. B. (**2013**). "GSAS II: the genesis of a modern open source all purpose crystallography software package," J. Appl. Crystallogr. **46**, 544–549.
Turner, M. J., McKinnon, J. J., Wolff, S. K., Grimwood, D. J., Spackman, P. R., Jayatilaka, D., and Spackman, M. A. (**2017**). *CrystalExplorer17*. (University of Western Australia). Available at: http://hirshfeldsurface.net.
van de Streek, J. and Neumann, M. A. (**2014**). "Validation of molecular crystal structures from powder diffraction data with dispersion-corrected density functional theory (DFT-D)," Acta Crystallogr. Sect. B: Struct. Sci., Cryst. Eng. Mater. **70**(6), 1020–1032.
Wang, J., Toby, B. H., Lee, P. L., Ribaud, L., Antao, S. M., Kurtz, C., Ramanathan, M., Von Dreele, R. B., and Beno, M. A. (**2008**). "A dedicated powder diffraction beamline at the advanced photon source: commissioning and early operational results," Rev. Sci. Instrum. **79**, 085105.
Wavefunction, Inc. (**2020**). Spartan '18 Version 1.4.5, Wavefunction Inc., 18401 Von Karman Ave., Suite 370, Irvine, CA 92612.
Wheatley, A. M. and Kaduk, J. A. (**2019**). "Crystal structures of ammonium citrates," Powd. Diffr. **34**, 35–43.